Forced Bonhoeffer–van der Pol oscillator in its excited mode

A. Rabinovitch,[1] R. Thieberger,[1,2] and M. Friedman[2]
[1]*Physics Department, Ben-Gurion University, Beer-Sheva 84105, Israel*
[2]*Physics Department, Nuclear Research Centre–Negev, Beer-Sheva P.O.B. 9001, Israel*
(Received 12 July 1993; revised manuscript received 4 January 1994)

A Bonhoeffer–van der Pol system is analyzed in the range of parameters where the attractor is a focus. The system's responses to a single pulse stimulus applied at different points along a "hidden structure" are used to construct a one-dimensional map from which the system's responses to pulse train stimulations are obtained.

PACS number(s): 87.22.Jb, 87.22.Fy, 87.10.+e

I. INTRODUCTION

The main concepts and the theoretical framework of biological oscillations have been extensively developed in recent years. These oscillations are analyzed by the limit cycle solutions of nonlinear differential equations. Since limit cycle solutions are periodic (with a time period T_0), the phase along the cycle is the fundamental time measuring property. The understanding of this phase and of its resetting following a perturbation constituted a major area of research [1] in nonlinear oscillators, one which had remarkable success in explaining numerous related biological phenomena.

There are biological problems, such as the response of a nerve axon to the passage of information, which can be analyzed by similar nonlinear equations but in a region where their solutions have a different character. In this region the solutions approach a final stable point, a focus. Since in this case no periodicity exists, the notions phase, phase resetting, etc. lose their meaning, and the theoretical framework mentioned above cannot be implemented.

In this paper we develop concepts and a framework for this region of solutions for a specific nonlinear equation (namely, the Bonhoeffer–van der Pol one). The use of this framework is then demonstrated in the analysis of the response of a nerve axon to a train of pulses given its response to a single pulse. The same method can be used in general to analyze other equations and systems where the differential equations are unknown but with similar characteristics (as was done in the limit cycle region).

The information passage through an axon can be modeled by a set of nonlinear differential equations. One of the best fitting sets is the well-known Hodgkin-Huxley [2] (HH) one. A simple approximation of a set of two equations is the Bonhoeffer–van der Pol system [3] (BVP), which retains a large portion of the topological features of the HH set. The parameters' values used for its neurophysiological applications restrict the phase space of the set to the following main mathematical characteristics: (a) There is only one attractor, in the region of interest, which is a focus. (b) The approach to the focus occurs along a hidden structure (HS), which is spiral in shape. (c) The flow to the focus from any initial point firstly approaches the HS and then continues alongside it. (d) There exists a specific curve [3–5] in phase space [see Fig. 1(a) below] called the separatrix, dividing the flow trajectories towards the HS, such that points on one side of the separatrix flow to one branch of the spiral while those on its other side flow to another branch. This feature provides a qualitative description of the "threshold mechanism" for a single pulse response of the physiological system. This mechanism is the well-known experimental phenomenon that pulses of amplitudes below a certain threshold value A_{th} fail to cause the axon to transport information, while pulses of the same duration

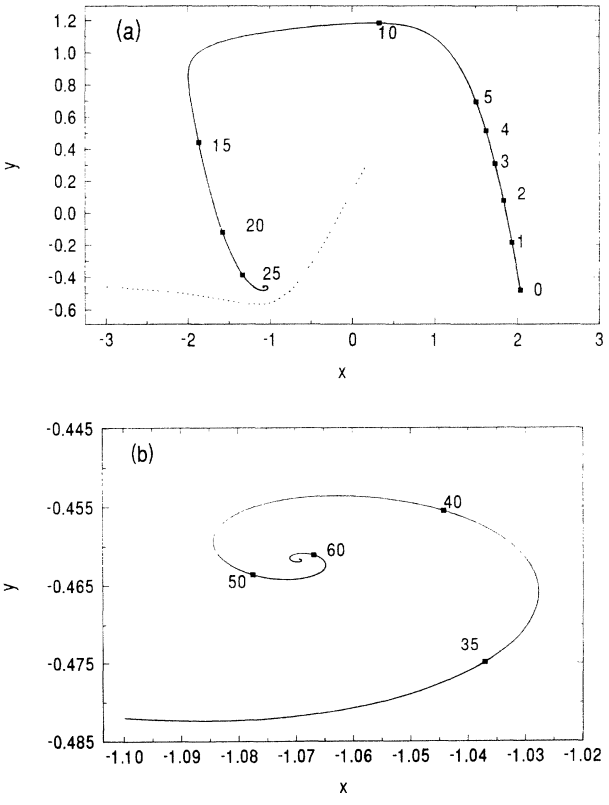

FIG. 1. The hidden structure and the separatrix, $A_0=0.2$. (a) Global behavior–the hidden structure for $0\le\tau\le25$. (b) Enlarged near-focus neighborhood.

with amplitudes higher than A_{th} do succeed in achieving it.

For most of the applications, a crossing of the separatrix which causes a large excursion of the trajectory in phase space, is considered to be a positive output (denoted by "1") while a noncrossing event is looked upon as a negative one (denoted by "0"). As we show below, this causes a distinction between a phase periodicity and an output periodicity for the HS case.

Biologically, an important feature of the system (axon), is its response to a train of pulses [6]. Such a train of pulses is characterized by two variables: the pulse strength S (given by its area), and the time interval T between consecutive pulses. Changing these variables, the global structure of the responses shows regions of phase locking and chaos. This global behavior was demonstrated recently both experimentally for a squid axon [7] and theoretically (or rather numerically) for the BVP set [4]. A somewhat similar behavior was obtained for the limit cycle case above a certain stimulus amplitude [8]. Mathematically, there are differences between the limit cycle and the HS cases. The main difference is derived from the limit cycle itself and causes every result there to be defined modulo the cycle period T_0; for the HS case, on the other hand, time increases monotonically to infinity as we approach the focus and no T_0 is defined (see a consequence which emphasizes this point in Sec. IV).

Since time along the HS is not defined modulo T_0 and is therefore not a phase, there exists no phase resetting response curves for this case. In the present paper we concentrate on the issue of defining and calculating the values of a similar relation, which we term a time resetting response curve (TRC). In a manner similar to the one used in the limit cycle case, we next show how to use the TRC to construct a one-dimensional (1D) map that gives the evolution of the times of kicks at different points along the HS. Iterations of this map are then shown to yield the system's dynamics under a train of pulses which are then compared with the direct integration of the differential equations.

As in the limit cycle case, this 1D map can be an extremely useful analytical tool. Using mapping theory methods for the limit cycle case (and for systems where no differential equation is known but which are supposed to be in a limit cycle situation), a better understanding of the biological systems has been gained [9]. We expect similar benefits for the HS case.

II. THE MODEL

The Bonhoeffer–van der Pol system is given by

$$\dot{x}=x-\frac{x^3}{3}-y+I(t)\ , \tag{1}$$

$$\dot{y}=c(x+a-by)\ . \tag{2}$$

In the neurophysiological application x is the axon's membrane potential, y is the refractivity, $I(t)$ is the input current, and a, b, and c are constants representing the membrane radius, the specific membrane fluid resistivity, and the temperature factor, respectively. In this paper we use similar values to those of Ref. [10], namely $a=0.7$, $b=0.8$, and $c=0.1$. Also, for a pulse train forcing

$$I(t)=A_0+A_1\sum_{m=0}^{\infty}\theta(t+d-mT)-\theta(t-d-mT)\ , \tag{3}$$

where $\theta(t)$ is the Heaviside step function, $A_0=0.2$ and $2d=0.3$ (the pulse width).

In order to characterize the hidden structure, initial points were chosen at different positions in phase space and their time evolutions under Eqs. (1) and (2) with $I(t)=A_0$ (no forcing) were calculated. Having obtained the HS, we located the point on its spiral section with minimum y and chose the point on its right-hand branch with the same y as the time origin [$\tau=0$; see Fig. 1(a)]. Starting from this point, the flow occurs exactly along the HS. Each point on the HS is now characterized by the time interval (τ) between zero and the time of arrival to this point (Fig. 1). Several points are to be noted.

(a) As the spiral radius decreases, the velocity along the HS obviously becomes smaller.

(b) The velocity is higher along the HS sections which are approximately parallel to the x axis than along the sections which are approximately parallel to the y axis.

(c) As the focus is approached, the time intervals needed to travel from, say, a point of minimum y to a point of maximum y converge to some constant value [$\delta\tau\sim 10$ in Fig. 1(b)]. This can easily be understood by linearizing Eqs. (1) and (2) around the focus (x_0,y_0):

$$\begin{aligned} x&=x_0+\xi\ ,\\ y&=y_0+\eta \end{aligned} \tag{4}$$

for small ξ and η. Recalling that $\dot{x}=\dot{y}=0$ at the focus, this linearization yields

$$\begin{aligned} \dot{\xi}&=(1-x_0^2)\xi-\eta\ ,\\ \dot{\eta}&=c(\xi-b\eta)\ . \end{aligned} \tag{5}$$

Let the eigenvalues of the Jacobian of Eq. (5) be $\lambda=-\alpha\pm i\omega$. For the parameters' values (a,b, etc.) used here, we have $x_0=-1.069$ and ($y_0=-0.462$) which provide $\alpha=0.111$ and $\omega=0.314$. Thus, the above mentioned time intervals approach $\pi/\omega\simeq 10$—the numerical value obtained.

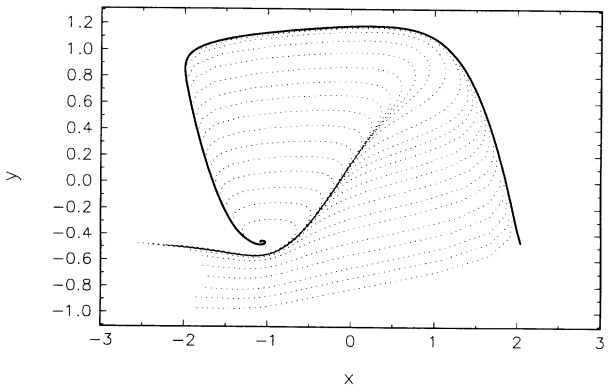

FIG. 2. The structure of the separatrix (heavy line) given as the inverse time contraction of several trajectories ($A_0=0.2$).

We have thus established a one to one correspondence between points on the HS and points on the positive time axis, which we define as the "internal time" τ. To obtain the separatrix [3] of Fig. 1(a), we took several initial points close to and within the HS boundaries and solved Eqs. (1) and (2) for $A_1=0$ (no pulses) with negative time. Results are shown in Fig. 2. The separatrix is seen to exist only to the right and bottom of the focus and to dwindle off for high values of y. In the region called "no man's land" by FitzHugh [3] (for $y \geq 0.5$), the separatrix is no longer discernible. We have to bear in mind that the separatrix is never a clear cut line such that points to its right behave completely differently than points to its left. Rather it can be looked upon as the line of maximum slope of the time excess (see Sec. III).

III. THE TIME EXCESS AND THE TRC

For each point P_1 along the HS, the time excess for a single pulse stimulus was calculated as follows: starting at P_1 as initial condition, Eqs. (1) and (2) were integrated assuming a single pulse of magnitude A_1 at P_1, i.e.,

$$I(t)=A_0+A_1[\theta(t)-\theta(t-2d)] \ . \tag{6}$$

The output is the trajectory from P_1 *with a pulse.* This trajectory eventually reapproaches the HS. We measured the distance of the P_1 trajectory from the HS, and when it became less than a prescribed tolerance ϵ, we marked its position P_2 (i.e., P_2 almost completely returned to the HS), and the time elapsed t_1. Had we started from P_1 along the HS (namely for $A_1=0$) we would have reached P_2 after a time interval t_2. We define the time excess as

$$\delta_{A_1}(P_1)=t_1-t_2 \ . \tag{7}$$

It measures the amount of time lost (or gained if $\delta<0$) by adding a pulse of height A_1 (or of strength $S=2dA_1$) at P_1.

This definition of the time excess holds whenever P_2 returns to the HS. It should be noted, however, that the separatrix which controls this return, exists only outside the inner spiral portion of the HS. Thus, if P_2 enters the inner spiral zone before returning to the HS, it will create its own spiral which converges to the same focus but at no time merges with the original one (continuation of the HS). In this case the time excess is defined as follows: after a reasonable transient period the first minimum on the new spiral is defined as P_2, and the closest minimum to P_2 on the HS (of the two possible ones) provides t_2.

A typical time excess map is given in Table I. The points along the HS are characterized by their τ values and the pulse heights—by A_1/A_{th}. The range of A_1/A_{th} values used in Table I is between 0.6 and 1.8, which is in accordance with the investigated values [4,6,7]. Lower values are biologically unimportant since no positive response is obtained there. In comparison, for the limit cycle case, even very small pulse amplitudes are interesting both theoretically (Arnold tongues, etc.) and experimentally.

TABLE I. Time excess map. $\delta(\tau)$ is calculated along the HS $A_1/A_{\text{th}}=0.6$, 0.9, 1.2, 1.5, and 1.8.

τ	0.6	0.9	1.2	1.5	1.8
2	0.	−0.05	−0.05	−0.05	−0.10
4	−0.05	−0.05	−0.10	−0.10	−0.15
6	0.15	0.20	0.20	0.25	0.25
8	0.70	0.90	1.10	1.20	1.35
10	0.35	0.55	0.85	1.10	1.45
12	0.05	0.10	0.10	0.15	0.15
14	0.10	0.10	0.15	0.20	0.20
16	0.10	0.15	0.25	0.30	0.35
18	0.20	0.25	0.35	0.45	0.60
20	0.30	0.50	0.70	0.90	1.10
22	0.65	1.05	1.45	1.90	2.40
24	1.50	2.40	3.30	4.30	5.40
26	−16.43	−14.23	7.30	8.85	12.65
28	−10.08	−9.18	12.30	32.75	30.75
30	−6.18	14.80	34.95	32.90	32.15
32	16.40	20.75	35.45	34.40	33.85
34	18.65	39.50	37.00	36.20	35.70
36	20.40	41.30	38.90	38.10	37.65
38	21.85	45.30	41.00	40.15	39.65
40	23.30	26.45	43.35	42.25	41.70
42	24.95	27.15	45.75	44.40	43.80
44	26.90	28.80	48.00	46.50	45.85
46	29.05	30.85	50.05	48.55	47.90
48	31.20	33.20	51.90	50.50	49.90
50	33.35	35.60	53.70	52.45	51.85

Several interesting qualitative conclusions can be gleaned from the table and from Fig. 3.

(1) For small τ's (points on the right branch of the HS), δ is small but negative. It means that it is faster to go from a to c through b [Fig. 3(a)] than directly along the HS. Apparently, the topographical slope along the $b-c$ route is much higher than the one along the ravine $a-c$.

(2) For P_1 close to the top of the HS, the return to the latter is very slow. Thus starting from, say, d or e, the flow is parallel to the HS (at some distance away) and the return occurs only after reaching the left side of the HS. This causes a relatively high δ values at $\tau \approx 9$. For higher values, say $\tau \approx 10-12$, P_1 is on top of the HS and the return occurs almost exactly along the HS (i.e., smaller δ).

(3) For P_1 on the left side of the HS ($\tau \sim$between 13 and 25), δ steadily increases, which implies that the slope along fgh, say, is not as large as that along abc.

(4) For specific A_1/A_{th} values (see, for example, Table I, $A_1/A_{\text{th}}=0.9$), a resonance effect occurs. We define here as resonance a large gain (or loss) of time due to geometrical effects. These are described in Fig. 3(b) for small values of A_1/A_{th} ($=0.4,0.6$): the pulse transfers a point on the HS to a location close enough to a *later* position on the HS, thus gaining time ($\delta<0$).

(5) The main feature of separatrix crossing can be seen, e.g., at point (i) ($\tau \approx 21$): for small A_1/A_{th}, the pulse is not strong enough to reach the separatrix and hence the return is relatively short timed (even though it is folded upon itself). For larger A_1/A_{th} values the return is done by an excursion through the right branch of the HS, resulting in a large increase of δ. It is to be noted, however,

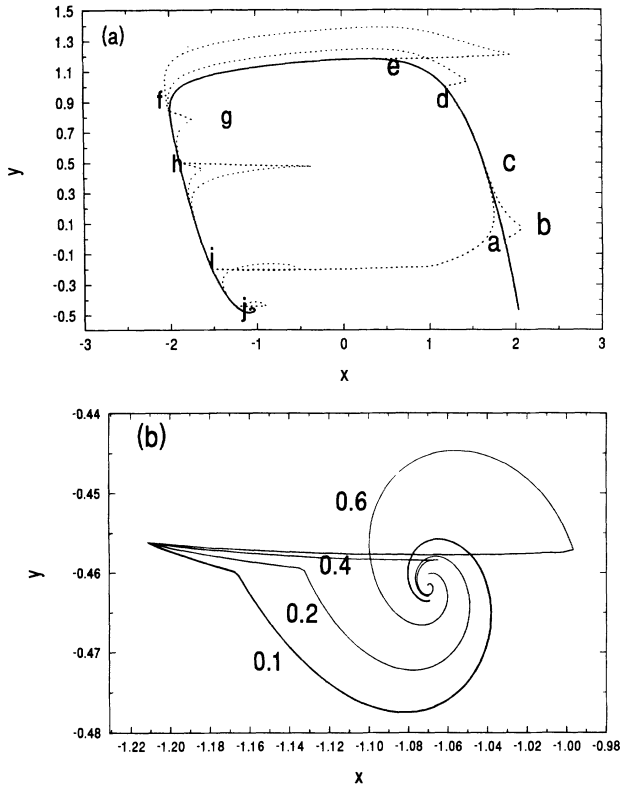

FIG. 3. Return to the HS. (a) Pulses (of different strengths) are applied at *a*, *d*, *e*, etc. At *i*, a weak pulse returns right back to the HS while a strong one is shown to have crossed the separatrix and returned to the HS near *c*. (b) Resonance behavior. Pulses of $A_1=0.4$ and 0.6 are shown to have gained significantly in time.

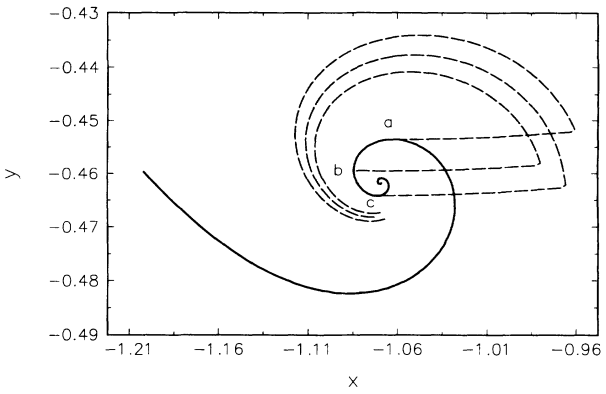

FIG. 4. Explanation of the linear increase of $\delta(\tau)$ for large τ. Pulses applied at *a*, *b*, and *c* all return approximately to the same location.

that the increase of δ as a function of A_1/A_{th} for the same τ is *not* a discontinuous one. The separatrix can therefore be defined only as the point where the slope of δ is a maximum.

(6) For sufficiently large A_1/A_{th}, and for P_1 within the inner spiral, $\delta(\tau)$ increases almost linearly. In Table I this effect holds for all A_1/A_{th} provided that τ exceeds 33. This can be explained as follows (Fig. 4): A sufficiently large pulse transfers all points with τ above some τ_0 into the same region. Therefore, the further inside in the spiral the initial point P_1 is, the larger is the time excess.

For each point P_1, characterized by τ, we have thus obtained the time excess $\delta_{A_1/A_{\text{th}}}(\tau)$. The eventual long time behavior of its trajectory could be obtained by starting on the HS with no forcing at

$$\tau'=\tau-\delta(\tau)\ . \tag{8}$$

This is the time-resetting curve (TRC). For each point it describes the apparent point of initiation on the HS which would give a similar asymptotic behavior when unforced.

Four examples of graphs of the time excess and the TRC are given in Fig. 5. These should be compared to the appropriate graphs for a forced limit cycle case (e.g., Fig. 3 of Ref. [8]). Note that in a repetitive operation (e.g., under a specific train of pulses), following a transient period, the TRC map becomes one to one which is very similar to the limit cycle case. The essential difference, however, is that the domain (and range) of this map is not constant as in the limit cycle case, but depends on the stimulus.

IV. PERIODIC STIMULATION

For a pulse train stimulation [Eq. (3)], Eqs. (1) and (2) can be integrated directly to yield the global structure of responses which contains phase locked regions of very specific types $[n/(n+1),n/(2n+1)]$ and chaotic regions [10] of the intermittency type.

An important point worth mentioning here is the basic difference between the HS and the limit cycle cases for long intervals (T) between consecutive pulses. For the HS case, beyond a certain value of T, the response is always "1;" that is, the system, having had enough time to relax, sees each pulse as a single stimulus. On the other hand, for the limit cycle case, there is a repetition of the bifurcation map each T_0, where T_0 is the limit cycle period. Thus, e.g., if for $T=T_1$ and for a certain A_1 the system is in a "1" region for the HS (or an equivalent "1:1" behavior for the limit cycle), for $T=T_1+T_0$ and for the same A_1, the HS system would still be in a "1" region, while the limit cycle system would move into a "1:2" region.

Here we wish to use the TRC of Sec. III to generate a map that could be exercised to obtain the pulse train response from the single pulse one. For the limit cycle case such a procedure has been studied extensively since 1964 [11].

The idea is to connect the internal time along the HS, when the nth, say, stimulus occurred (τ_n), to the internal time of occurrence of the previous stimulus (τ_{n-1}). The input time interval between two consecutive pulses is T, and we assume that T is large enough for the trajectory to have almost completely returned to the HS. For a

very fast pulse repetition rate (very small T), a completely different behavior is obtained.

At τ_{n-1} the system suffered a stimulus which caused its internal time to be reset to τ'_{n-1} [Eq. (8)]. The next pulse occurs one time interval T later, hence $\tau_n=\tau'_{n-1}+T$, or

$$\tau_n=f(\tau_{n-1})=\tau_{n-1}-\delta(\tau_{n-1})+T \ . \tag{9}$$

This is the desired 1D map. It controls the pulse train response, as we will presently demonstrate.

In the following discussion we distinguish between two cases: mode locking and chaotic response.

A. Mode locking

A necessary condition for a periodic output of any type is that a specific iteration of the map [Eq. (9)] will satisfy (*phase periodicity*)

$$\tau_{n+p}=\tau_n \ , \tag{10}$$

$$\tau_{n+m}\neq\tau_n, \quad m<p \tag{11}$$

for some integers n and p. Such a period-p output does not completely define the response. In order to understand this point consider a period-3 case. For the neurophysiological result this case can be characterized by two distinct sequences of pulse-outputs: "100" and "110," depending on the number of times (one or two, respectively), during a complete period of $3T$, that the separatrix has been crossed and a large excursion around the whole of the HS has occurred. These distinct sequences are called output periodicities. Note that a "111" case is excluded by Eq. (11), while "000" is always regarded as a zero response. When the system is in a zero response region, the actual phase space trajectory is usually periodic. The radius of its shape, however, is smaller than the outer radius of the HS. Although such movements are usually without any biological significance, they are topologically interesting since they are specific to the spiral HS case with no counterpart for that of the limit cycle.

Since a "10" response is the only period-2 case possible, we begin by analyzing the conditions for this case. The second iteration $f^2(\tau_n)$ was calculated for a specific $A_1/A_{\rm th}$ value and for several values of T. The limits of

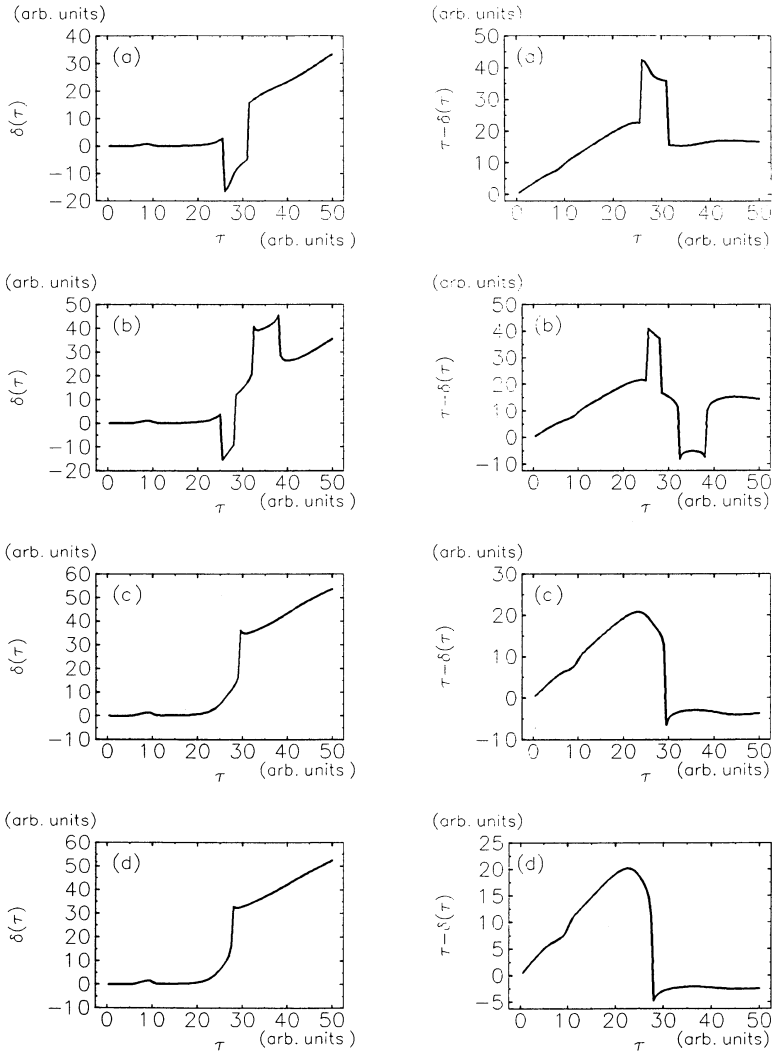

FIG. 5. Time excess $[\delta(\tau)]$ and time resetting $[\tau-\delta(\tau)]$ curves. $A_0=0.2$, and $A_1/A_{\rm th}=0.6$ [(a),(b)], 0.9 [(c),(d)], 1.2 [(e),(f)], and 1.5 [(g),(h)]. To obtain the map [Eq. (9)] move the TRC upwards by T.

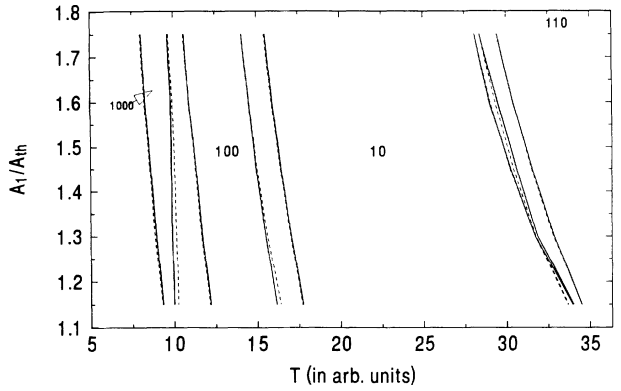

FIG. 6. Mode-locked regions ($A_0=0.2$). The calculated boundaries are obtained from the differential system [Eqs. (1)–(3)], while the predicted ones are derived from the map [Eq. (9)].

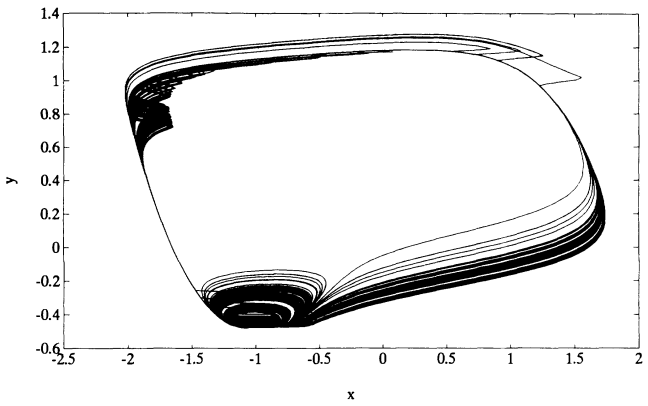

FIG. 8. Phase-space appearance of a chaotic trajectory. $A_0=0.2$, $A_1/A_{th}=1.3$, and $T=15.65$.

the interval of T values for which a solution to $f^2(\tau_n)=\tau_n$ is possible [but no solution of $f(\tau_n)=\tau_n$] mark the predicted limits of the "10" region for this A_1/A_{th} value. Once the "10" region was determined, other regions such as "100," "110," etc. were similarly calculated. Note that a period-3 solution occurring to the right of the "10" region implies a "110" case, while a solution of the same periodicity appearing on the left of the "10" region signals a "100" case. Results are shown in Fig. 6, where the different predicted [i.e., obtained from Eq. (9)] zones are compared with those calculated directly from the differential system [Eqs. (1–3)]. The agreement is excellent and depends only on the accuracy of the numerical calculations.

Since Eq. (9) predicts the exact τ's where the stimuli occur (following a certain transient time), and since these τ' are in a one- to- one correspondence with positions along the HS (Sec. II), these positions can be compared immediately with the ones obtained directly by Eqs. (1)–(3). Two such comparisons are shown in Fig. 7. The cases $A_1/A_{th}=1.6$ and $T=12$ and 30, shown in Figs. 7(a) and 7(b) respectively, are—according to Fig. 6— in the "100" and "110" zones. We thus calculated the exact solutions to $f^3(\tau_n)=\tau_n$ for both cases and compared them to the phase-space solutions of Eqs. (1)–(3). Once again, there is a very good agreement.

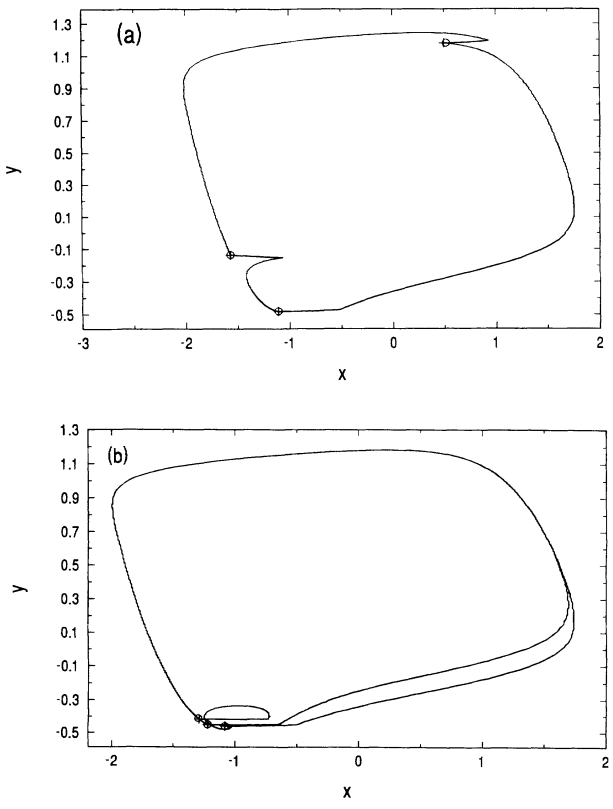

FIG. 7. Phase-space pulse positions. $A_0=0.2$, $A_1/A_{th}=1.6$. The predicted positions (+) are obtained by Eq. (9) and Fig. 1, and the calculated ones (○) by Eqs. (1)–(3). (a) $T=12$, "100" case. (b) $T=30$, "110" case.

B. Chaotic response

For some regions of the $A_1/A_{th}-T$ plane, chaotic behavior has been observed both experimentally for the squid axon [6,7] case and theoretically for the BVP [4]. A typical chaotic phase-space response is shown in Fig. 8. In order to obtain the chaotic bifurcation scheme from the time excess map, we iterated Eq. (9) several hundred

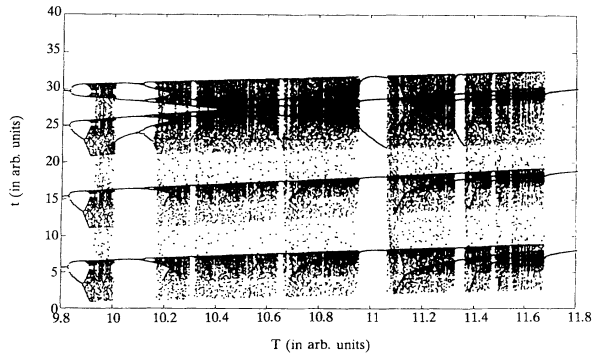

FIG. 9. Bifurcation diagram for $A_0=0.2$, $A_1/A_{th}=1.3$. It is obtained by recording several hundred consecutive iterations of Eq. (9) after deleting the first transient ones.

times, following a transient period, at a fixed value of A_1/A_{th} (=1.3) and for a whole range of T values. The results are shown in Fig. 9. Note that the values plotted are those of τ_n's, while had we used the differential system these would have been x_n's or y_n's. The T values in Fig. 9 traverse the range between "10^3" and "10^2." The onset of chaos at around $T=9.88$ is achieved via a period-doubling cascade, while the transition to "10^2" at around $T=11.68$ occurs abruptly. The overall behavior is in good agreement with the results discussed in Ref. [10].

V. CONCLUSIONS

A time-resetting curve method has been developed for a system in the state where its attractor is a focus and the approach to the focus is via a hidden spiral structure. This situation, being different topologically from the limit cycle one which has been analyzed extensively hitherto, shows some unique properties. We have demonstrated the applicability of the method to the BVP system in the range where it is used, e.g., for the analysis of the response of an axon to a stimulation by a train of pulses. Since the use of the mapping [Eq. (9)] makes the analysis of mode locked and chaotic behaviors simpler, both qualitatively and quantitatively, than the original differential equations, and since mapping techniques are the only ones available in many experimental situations where no differential equation is known, we hope that the TRC will become a useful tool in the treatment of such systems, much as its counterpart, the phase resetting curve method, has become for problems of the limit cycle type.

[1] A. T. Winfree, *The Geometry of Biological Time* (Springer-Verlag, New York, 1980); L. Glass and M. C. Mackey, *From Clocks to Chaos* (Princeton University Press, Princeton, 1988).

[2] J. Cronin, *Mathematical Aspects of Hodgkin-Huxley Neural Theory* (Cambridge University Press, Cambridge, 1987).

[3] R. FitzHugh, J. Gen. Physiol. **43**, 867 (1960), Biophys. J. **1**, 445 (1961); M. Okuda, Prog. Theor. Physiol. **66**, 90 (1981).

[4] M. Friedman, A. Rabinovitch, and R. Thieberger (unpublished).

[5] H. Treutlein and K. Schulten, Eur. Biophys. J. **13**, 355 (1986), Ber. Bunsenges. Phys. Chem. **89**, 710 (1985).

[6] G. Matsumoto, K. Aihara, Y. Hanyu, N. Takahashi, S. Yoshizawa, and J-i Nagumo, Phys. Lett. **123A**, 162 (1987).

[7] N. Takahashi, Y. Hanyu, T. Musha, R. Kubo, and G. Matsumoto, Physica **34D**, 318 (1990).

[8] W.-Z. Zeng, M. Courtemanche, L. Sehn, A. Shrier, and L. Glass, J. Theor. Biol. **145**, 225 (1990).

[9] Phase resetting methods have been used in many systems (Ref. [1]). Other examples are the analyses of respiratory systems [e.g., J. Lewis, M. Bachoo, L. Glass, and C. Polosa, J. Theor. Biol. **159**, 491 (1992)], mastication [e.g., J. P. Lund, S. Rossignol, and T. Murakami, Can. J. Physiol. Pharmacol. **59**, 683 (1981)], diagnosis of Parkinsonism [e.g., R. G. Lee and R. B. Stein, Ann. Neurol. **10**, 523 (1981)], and clinical applications of modulated parasystolic rhythms [see, e.g., the review by J. Jalife and D. C. Michaels, in *Cardiac Electro Physiology and Arrythmias*, edited by D. P. Zipes and J. Jalife (Grune and Stratton, Orlando, FL, 1985)], p. 109 ff.

[10] S. Yasin, M. Friedman, S. Goshen, A. Rabinovitch, and R. Thieberger, J. Theor. Biol. **160**, 179 (1993).

[11] D. H. Perkel, J. H. Schulman, T. H. Bullock, G. P. Moore, and J. P. Segundo, Science **145**, 61 (1964), and see Ref. [1] for a whole list of references.

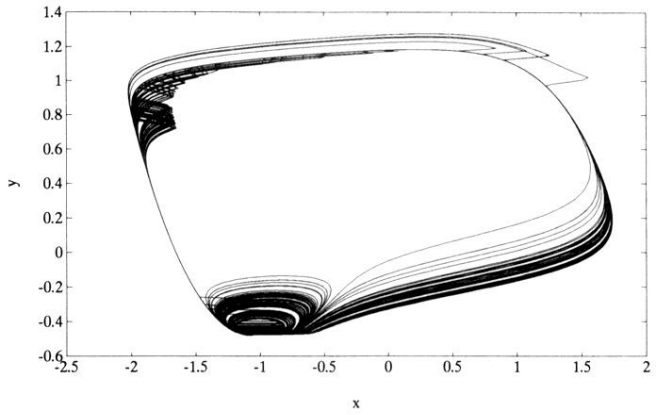

FIG. 8. Phase-space appearance of a chaotic trajectory. $A_0=0.2$, $A_1/A_{\text{th}}=1.3$, and $T=15.65$.

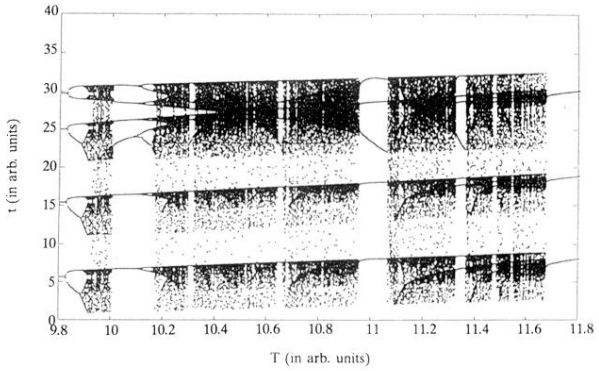

FIG. 9. Bifurcation diagram for $A_0 = 0.2$, $A_1 / A_{th} = 1.3$. It is obtained by recording several hundred consecutive iterations of Eq. (9) after deleting the first transient ones.